Int. J. Heat Mass Transfer. Vol. 35, No. 5, pp. 1169–1180, 1992
Printed in Great Britain

0017-9310/92 $5.00 + 0.00

Removal of contaminant generated by a discrete source in a slot ventilated enclosure

J. L. LAGE and A. BEJAN
Department of Mechanical Engineering and Materials Science, Duke University, Durham, NC 27706, U.S.A.

and

R. ANDERSON
SERI, Building Energy Technology Program, 1617 Cole Boulevard, Golden, CO 80401, U.S.A.

(*Received* 22 *February* 1991 *and in final form* 3 *May* 1991)

Abstract—This paper reports the results of a numerical study of the time-dependent removal of contaminant from a two-dimensional enclosure with one inlet and one outlet. The contaminant is generated beginning with the time $t = 0$ by a concentrated source located inside the enclosure. The contaminant is removed by the through flow established between the inlet and outlet ports. The flows studied cover the laminar and turbulent regimes represented by $30 \leqslant Re \leqslant 3000$, where Re is the Reynolds number based on the inlet width and mean velocity. The effectiveness of the contaminant removal scheme is documented in terms of the removal efficiency η_r, the volume-averaged concentration of contaminant $\bar{C}$, and the critical (clean up) time t_c. The effects of Re, ventilation jet orientation and source location are reported. It is shown that the movement and distribution of contaminant is complex and depends strongly on the source location. It is also shown how the relative positioning of the ports and the source location influence the contaminant removal process. The optimal inlet/outlet configuration associated with each position of the concentrated source of contaminant is reported. Slower ventilation schemes can lead to lower contaminant levels when a short contaminant removal time is not a major requirement.

1. INTRODUCTION

THE MOVEMENT of indoor air, and the distribution of contaminants through living spaces have attracted considerable attention during the last decade. The 'sick building' syndrome is now seen as a factor in the decrease of productivity and worker performance in enclosed work spaces.

The competing requirements of conserving energy in a building, and improving the quality of indoor air have made mandatory the search for efficient ventilation schemes. Two distinct components of ventilation engineering are of interest: (1) the mechanical system that produces the air flow (compressors, fans, ducts, etc.), and (2) the architectural configuration of the flow system (inlet and outlet positions and dimensions, room partitions, etc.).

The present study addresses the second component, and focuses on a fundamental problem in the conceptual design of any ventilation flow scheme. That problem is the removal of a contaminant that is being steadily generated by a concentrated source placed at a point inside the room. It is an important problem because its results show the engineer not only how to best design the contaminant removal flow scheme, but also the contaminant levels that can be expected to persist in the room in the steady state. This second aspect is essential if people are to be able to coexist with the contaminant source in the same room.

2. MODEL

The two-dimensional enclosure that forms the subject of this study is shown in the upper frame of Fig. 1. A discrete source of contaminant is located inside the enclosure, at a point whose position can be changed from one phase of the study to the next. The fluid mixture (base fluid + contaminant) is modelled as a Newtonian fluid with constant density and viscosity. The mass diffusivity (D) for the diffusion of contaminant through the mixture is also treated as constant.

The governing equations are the Reynolds-averaged equations for mass continuity, momentum and species conservation. The concentration equation retains the time-derivative term since the averaging is taken only over the high frequencies associated with turbulent fluctuations. It accounts for the much slower development of the mixing flow initiated through the enclosure. As indicated in Fig. 1, a 'clean' and steady through flow $\dot{m}$ is imposed. At time $t = 0$, a point mass source begins to generate contaminant inside the cavity.

The dimensionless time-averaged equations for

NOMENCLATURE

$a_{1,2,k}$	constants, equation (18)
B	source term, equation (10)
c	concentration [kg m^{-3}]
C	dimensionless concentration, equation (12)
D	mass diffusivity
E	dimensionless rate of dissipation of turbulence kinetic energy
$f_{1,2}$	dimensionless factors, equations (15) and (16)
G	turbulence kinetic energy due to viscous stress, equation (9)
h	width of inlet and outlet ports
H	height of enclosure
k	turbulence kinetic energy
K	dimensionless turbulence kinetic energy, equation (12)
L	length of enclosure
$\dot{m}$	mass flow rate, Fig. 1
$\dot{m}_s'''$	source mass flow rate per unit of volume [kg m^{-3} s^{-1}]
$\dot{M}_s$	source mass flow rate, equation (14)
p	pressure
P	dimensionless pressure, equation (13)
P_K	turbulence kinetic energy due to Reynolds shear stresses, equation (8)
q	source volumetric flow rate [m^3 s^{-1}]
Q	inlet volumetric flow rate [m^3 s^{-1}]
Re	Reynolds number based on inlet width, equation (14)
Re^*	Reynolds number based on eddy viscosity, equation (14)
Re_t	turbulence Reynolds number, equation (17)
Sc	molecular Schmidt number, ν/D
t	time
t_c	critical concentration decay time, equation (27)
u	horizontal velocity
u_{in}	average inlet velocity
U	dimensionless horizontal velocity, equation (11)
V	enclosure volume
v	vertical velocity
V	dimensionless vertical velocity, equation (11)
x	horizontal coordinate
X	dimensionless horizontal coordinate, equation (11)
y	vertical coordinate
Y	dimensionless vertical coordinate, equation (11).

Greek symbols

$\alpha_{x,y}$	grid stretching rates, Tables 1 and 2
$\Delta_{x,y}$	line-to-line spacing near boundary, Tables 1 and 2
ε	rate of dissipation of turbulence kinetic energy
η_r	removal efficiency, equation (23)
ν	kinematic viscosity
ν_t	turbulence kinematic viscosity
ρ	density
σ_C	turbulence Schmidt number
$\sigma_{\varepsilon,K}$	turbulence Prandtl numbers
τ	dimensionless time, equation (11)
τ^*	dimensionless time, equation (21)
τ_c^*	critical dimensionless time, equation (26)
Ψ	dimensionless streamfunction.

Subscripts and superscript

in	inlet
out	outlet
max	maximum
s	related to source
$\bar{}$	space averaged.

mass, momentum and species conservation are

$$\frac{\partial U}{\partial X}+\frac{\partial V}{\partial Y}=0 \tag{1}$$

$$U\frac{\partial U}{\partial X}+V\frac{\partial U}{\partial Y}=-\frac{\partial P}{\partial X}+\frac{1}{Re}\nabla^2 U+2\frac{\partial}{\partial X}\left(\frac{1}{Re^*}\frac{\partial U}{\partial X}\right)+\frac{\partial}{\partial Y}\left[\frac{1}{Re^*}\left(\frac{\partial V}{\partial X}+\frac{\partial U}{\partial Y}\right)\right] \tag{2}$$

$$U\frac{\partial V}{\partial X}+V\frac{\partial V}{\partial Y}=-\frac{\partial P}{\partial Y}+\frac{1}{Re}\nabla^2 V+\frac{\partial}{\partial X}\left[\frac{1}{Re^*}\left(\frac{\partial V}{\partial X}+\frac{\partial U}{\partial Y}\right)\right]+2\frac{\partial}{\partial Y}\left(\frac{1}{Re^*}\frac{\partial V}{\partial Y}\right) \tag{3}$$

$$\frac{\partial C}{\partial \tau}+U\frac{\partial C}{\partial X}+V\frac{\partial C}{\partial Y}=\frac{1}{Re\,Sc}\nabla^2 C+\nabla\cdot\left(\frac{\nabla C}{Re^*\sigma_c}\right)+\dot{M}_s. \tag{4}$$

The last term in equation (4) accounts for the generation of species inside the enclosure. This term is zero everywhere except at the point where the source is located.

The eddy diffusivity was evaluated based on Jones and Launder's [1] low Reynolds number k–ε model, which consists of solving two additional equations

$$U\frac{\partial K}{\partial X}+V\frac{\partial K}{\partial Y}=\frac{1}{Re}\nabla^2 K+\nabla\cdot\left(\frac{\nabla K}{Re^*\sigma_K}\right)+P_K+G-Re\,E \tag{5}$$

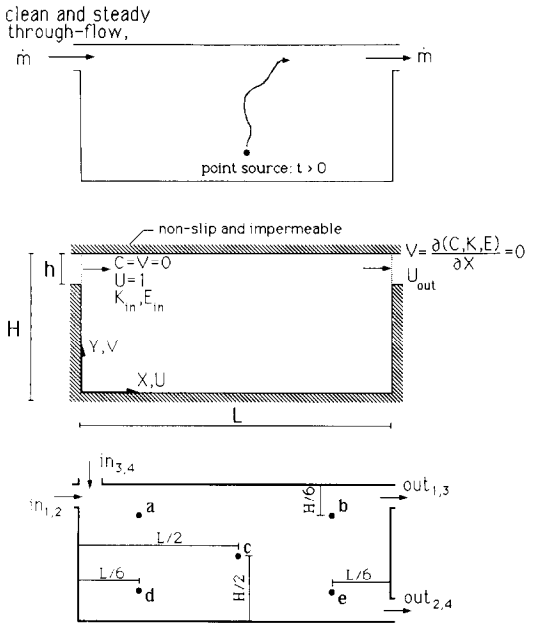

FIG. 1. Two-dimensional enclosure with steady through flow (top), dimensionless boundary conditions (middle), source locations and inlet/outlet configurations (bottom).

$$U\frac{\partial E}{\partial X}+V\frac{\partial E}{\partial Y}=\frac{1}{Re}\nabla^2 E+\nabla\cdot\left(\frac{\nabla E}{Re^*\sigma_E}\right)+a_K P_K\frac{E}{K}+B-a_1 f_1 Re\frac{E^2}{K} \quad (6)$$

in which

$$\nabla=\frac{\partial}{\partial X}\mathbf{i}+\frac{\partial}{\partial Y}\mathbf{j} \quad (7)$$

and

$$P_K=\frac{1}{Re^*}\left\{2\left[\left(\frac{\partial U}{\partial X}\right)^2+\left(\frac{\partial V}{\partial Y}\right)^2\right]+\left(\frac{\partial U}{\partial X}+\frac{\partial V}{\partial Y}\right)^2\right\} \quad (8)$$

$$G=-\frac{2}{Re}\left[\left(\frac{\partial}{\partial X}K^{1/2}\right)^2+\left(\frac{\partial}{\partial Y}K^{1/2}\right)^2\right] \quad (9)$$

$$B=\frac{2}{Re^2\,Re^*}\left[\left(\frac{\partial^2 U}{\partial Y^2}\right)^2+\left(\frac{\partial^2 V}{\partial X^2}\right)^2\right]. \quad (10)$$

Physically, P_K accounts for the production of kinetic energy by Reynolds shear stresses, while G represents the kinetic energy generated by viscous stresses. As indicated by Jones and Launder, equation (10) does not have a physical interpretation: B is a source term required in order to match turbulence kinetic energy to experimental data. Another feature of the Jones and Launder low Reynolds number model [1] is that it does away with the need for the wall functions used in more conventional k–ε models. Although other models are available, the Jones and Launder model was chosen because it is used more widely in computational fluid dynamics.

The writing of equations (1)–(4) is based also on the assumption that the source mass flow rate is negligible when compared with the mass flow rate of the through flow $\dot{m}$. Equations (1)–(10) have been written in terms of the following dimensionless variables:

$$(X, Y)=\frac{(x, y)}{h},\quad (U, V)=\frac{(u, v)}{u_{in}},\quad \tau=\frac{u_{in}}{h}t \quad (11)$$

$$C=\frac{(c-c_0)Q}{c_s q},\quad K=\frac{k}{u_{in}^2},\quad E=\frac{\nu}{u_{in}^4}\varepsilon \quad (12)$$

$$P=\frac{P}{\rho u_{in}^2},\quad Sc=\frac{\nu}{D},\quad \dot{M}_s=\frac{\dot{m}_s'''}{\frac{qc_s}{Q}\frac{u_{in}}{h}} \quad (13)$$

$$Re=\frac{u_{in}h}{\nu},\quad Re^*=\frac{u_{in}h}{\nu_t}=\frac{Re}{a_2 f_2}\frac{E}{K^2} \quad (14)$$

in which on the right-hand side we see the actual (physical) variables listed in the Nomenclature. Worth mentioning are the Reynolds number based on inlet width, Re, and the relationship between Re and Re^*, equation (14). The dimensionless factors f_1 and f_2 are functions of only the turbulence Reynolds number Re_t defined in equation (17)

$$f_1=1-0.3\exp(Re_t^2),\quad f_2=\exp\left[\frac{-2.5}{1+Re_t/50}\right] \quad (15, 16)$$

$$Re_t=\frac{k^2}{\nu\varepsilon}=\frac{K^2}{E}. \quad (17)$$

The numerical constants required by this model were selected using the approach described by Patankar *et al.* [2]. The numerical values of these constants are the same as those proposed by Jones and Launder [1]

$$a_k=1.44,\quad a_1=1.92,\quad a_2=0.09$$
$$\sigma_K=1,\quad \sigma_E=1.3 \quad (18)$$

except for the turbulent Schmidt number, which was set at $\sigma_C=0.7$. This value of σ_C was determined optimally in an earlier study [3] in which we used the present model to simulate the once-through removal of contaminated air from a two-dimensional enclosure. In that earlier study, we selected the σ_C value by comparing the numerical predictions with the laboratory measurements reported by Anderson and Mehos [4]. It is also worth noting that $\sigma_C=0.7$ lies between the 0.5 value associated with the free jet flow, and the 0.9 value found in turbulent boundary layers.

The boundary conditions are shown in the center frame of Fig. 1. The no-slip impermeable condition is imposed on all the solid walls. The flow through the inlet port is purely horizontal (forming a wall jet along the ceiling), and the velocity and concentration of this stream are uniform over the cross-section of the inlet

port. The inlet concentration is the same as the enclosure concentration at $\tau = 0$. The dimensionless values of K and E at the inlet are based on the assumption of fully developed turbulent flow, in which k represents 1% of the mean kinetic energy, and where the representative mixing length is of the order of 5% of the inlet width h

$$K_{in} = 0.01, \quad E_{in} = \frac{0.02}{Re}. \tag{19}$$

The outlet boundary condition (zero flux, Fig. 1) was chosen for numerical convenience. Nevertheless, its validity was verified by numerical tests performed at the low Reynolds number end of this study, $Re = 30$, since only in the low Re limit the outlet boundary condition is expected to have some influence on the upstream field. In these tests, the concentration was specified (held fixed) in the plane of the outlet port. The value of the outlet concentration was two times greater than the maximum outlet concentration calculated with the zero flux boundary condition. There was no difference between the upstream concentration field calculated with the fixed outlet concentration, and the one based on the zero flux outlet condition. The influence of the outlet boundary condition is expected to be even less significant for the higher Reynolds number documented in the present study. The zero-mass flux condition at the outlet has been used in other studies of forced convection heat and mass transfer, for example, in refs. [2, 5–8].

The shape of the enclosure and the relative size of the two ports (one inlet, one outlet) were fixed

$$\frac{L}{H} = 2, \quad \frac{h}{H} = 0.1. \tag{20}$$

In view of the range covered by the mass diffusivity of gases in air at 25°C and 1 atm, the molecular Schmidt number was set equal to 1 throughout the calculations performed in this study.

As an alternative to the dimensionless time τ defined in equation (11), it is useful to define the volume replacement time

$$\tau^* = \frac{t}{LH/u_{in}h}. \tag{21}$$

The quantity in the denominator represents the time in which the inlet stream can fill the enclosure volume. The proportionality between the dimensionless times τ^* and τ is

$$\frac{\tau^*}{\tau} = \frac{h^2}{LH} \tag{22}$$

or, according to equations (20), $\tau^* = 0.005\tau$. The gradual removal of the contaminant from the enclosure was monitored by calculating the 'removal efficiency' introduced by Anderson and Mehos [4]

$$\eta_r = \frac{1}{\tau}\int_0^\tau \frac{(c_{out} - c_{in})Q}{c_s q}\,dt = \frac{1}{\tau}\int_0^\tau C_{out}\,dt. \tag{23}$$

Also monitored was the volume-averaged pollutant concentration

$$C = \frac{1}{LH}\int_V C\,dV \tag{24}$$

in which $V = LH$ is the enclosure volume per unit length in the direction perpendicular to the plane of Fig. 1.

The lower frame of Fig. 1 shows the five different locations (a–e) of the contaminant source. These positions were chosen in order to document the effect of source location on contaminant removal. The lower frame of Fig. 1 also shows the four inlet/outlet configurations studied. Those are indicated by subscripts 1–4.

3. NUMERICAL METHOD

The equations described in the preceding section were solved numerically using the control volume formulation described by Patankar [9]. The steady momentum equations were solved by a false unsteady scheme. It was assumed that the steady state was reached when the maximum local relative change in the velocity components (U, V) was smaller than 10^{-3}.

The species transport equation was solved iteratively. At every time step the correspondent algebraic equation was invoked on a line-by-line basis using the Tri-Diagonal-Matrix-Algorithm (TDMA). This process was repeated until the solution converged. The convergence criterion was a global one based on the relative incremental changes in the removal efficiency

$$\frac{\eta_r^{j+1} - \eta_r^j}{\eta_r^j} < 10^{-6}. \tag{25}$$

The reported numerical results were obtained using the Cornell National Supercomputer Facility (CNSF) mainframe, which is an IBM 3090-600J computer. The code was highly vectorized in order to reduce the CPU time, especially while solving the higher Reynolds number cases.

The numerical grid for solving the flow field was orthogonal and non-uniform, with its lines spaced according to the power law $s_{i+1} = s_i + \alpha^i\Delta$, in which Δ is the size of the first line-to-line spacing (near the boundary), i the line number, and α (a constant greater than 1) the grid stretching rate. The appropriate grid spacing was selected based on accuracy tests of the kind shown in Table 1. The minimum streamfunction

Table 1. Accuracy test for the reference configuration (the top frame of Fig. 1, with $Re = 3000$)

$N_x \times N_y$	Δ_x/Δ_y	α_x/α_y	Ψ_{min}	CPU (s)
62×42	0.075/0.0375	1.089/1.172	−0.3738	2806
72×52	0.050/0.0250	1.087/1.147	−0.3802	3993
82×62	0.025/0.0125	1.097/1.146	−0.3821	5307

Table 2. Accuracy test for the reference configuration (Fig. 1, top), with the source located in the center of the enclosure (Fig. 1, bottom, position c), and $Re = 3000$

$N_x \times N_y$	$\Delta_x = \Delta_y$	α_x/α_y	$\Delta\tau$	$\bar{C}_{max}$ $(\tau \to \infty)$	CPU (s)
82×62	0.020	1.105/1.122	0.10	46.027	782
110×82	0.010	1.087/1.105	0.05	47.489	1280
142×102	0.005	1.074/1.096	0.01	47.908	2265

$\Psi_{min} = \min[\Psi(X, Y)]$ was used as a parameter, where Ψ was defined by writing $U = \partial\Psi/\partial Y$ and $V = -\partial\Psi/\partial X$. The present numerical results were obtained using the 82×62 grid.

A multigrid was employed in order to predict accurately the concentration field. A fine non-uniform power law grid located around the control volume containing the point source was superimposed on the grid used to calculate the flow field. Several accuracy tests for the different configurations used in this study were performed. The optimum arrangement was found by reducing the grid size and time step until a discrepancy smaller than 2% in the steady-state maximum volume-averaged pollutant concentration was found. Table 2 shows some of the results and the corresponding computation CPU time. The last row shows the values used throughout this study.

4. THE REFERENCE CONFIGURATION

Figure 2 presents the steady-state flow field in the reference configuration in which the inlet and outlet ports are parallel and near the ceiling of the enclosure (Fig. 1, top). The same configuration carries the subscript 1 in the bottom drawing of Fig. 1. The Reynolds number covers the range from the laminar regime ($Re = 30$) to that of the turbulent wall jet flow ($Re = 3000$). The numbers listed next to the streamlines represent the values of the dimensionless streamfunction Ψ defined in the preceding section.

The common feature of these three plots is the presence of a clockwise rotating cell in the lower portion of the enclosure. As the Reynolds number increases, a weak counter-clockwise cell develops in the lower left corner, while the incoming jet stretches (becomes straighter and thinner) near the ceiling of the enclosure.

The next five figures, Figs 3–7, show the Reynolds number effect on the steady-state distribution of contaminant, for each of the five source locations. The constant-concentration lines are plotted so that from one line to the next the C value changes by one tenth of the maximum concentration value. Some C values are included for orientation. Listed on each frame is

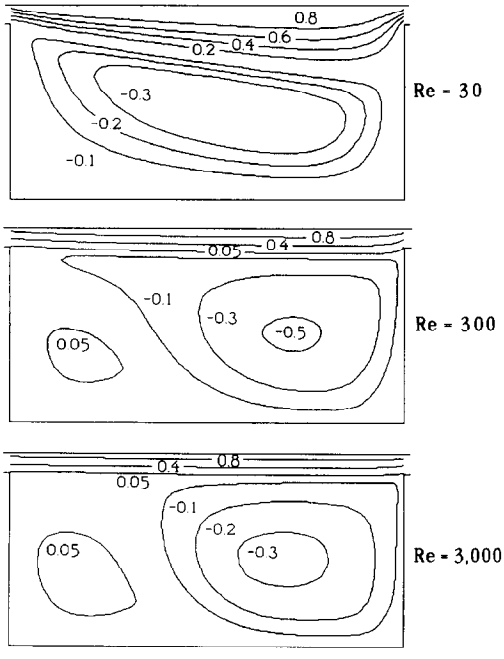

FIG. 2. The steady-state flow field for inlet/outlet configuration 1 and different Reynolds numbers.

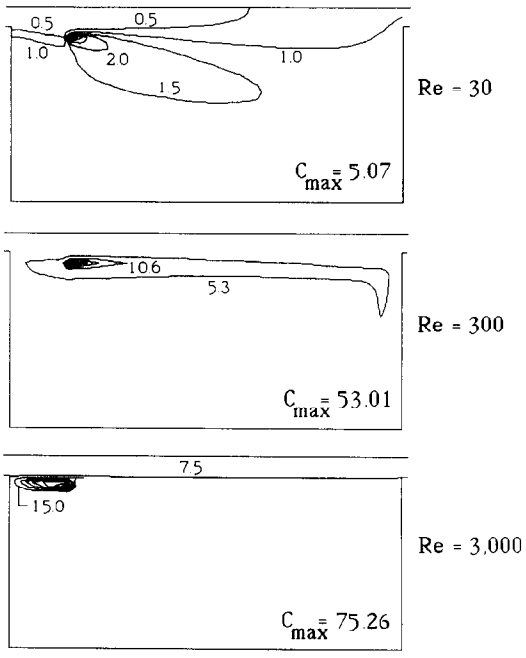

FIG. 3. The steady-state concentration field for source location a and configuration 1.

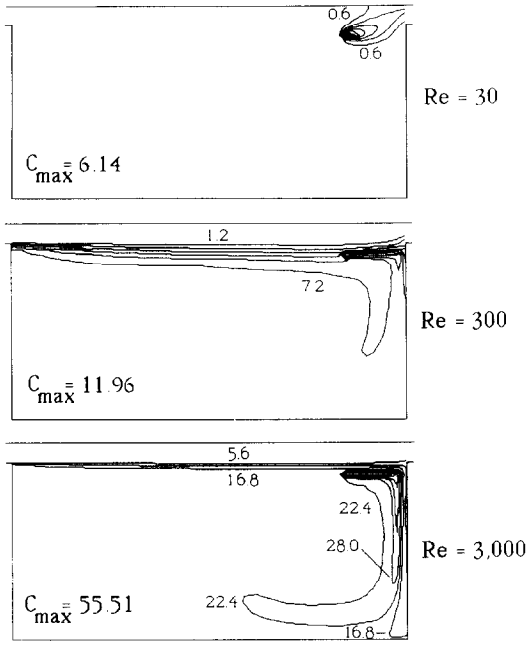

FIG. 4. The steady-state concentration field for source location b and configuration 1.

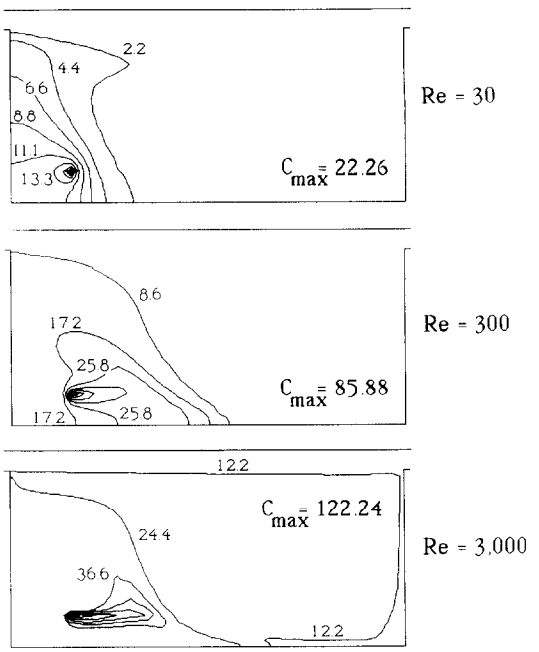

FIG. 6. The steady-state concentration field for source location d and configuration 1.

the maximum concentration value computed inside the enclosure, near the source (C_{max}).

The time evolution of the concentration field is illustrated in Fig. 8 for the case when the source is located in the center of the enclosure ($Re = 3000$). Note how the flow traps the contaminant in the lower-right region of the enclosure. Inside the jet region (near the ceiling) the pollutant concentration is always lower than 10% of the maximum concentration found in the enclosure. This is due to the fact that the incoming clean air bypasses the rest of the enclosure, and proceeds directly toward the outlet.

The contaminant removal efficiency η_r defined in equation (23) is reported in Fig. 9. The upper frame

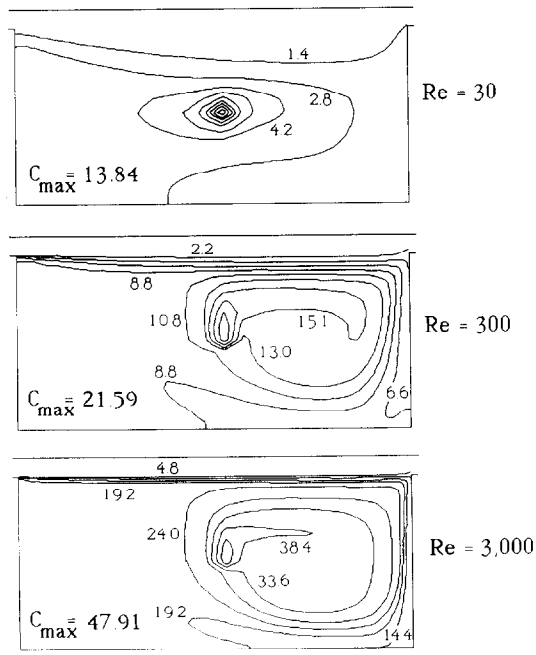

FIG. 5. The steady-state concentration field for source location c and configuration 1.

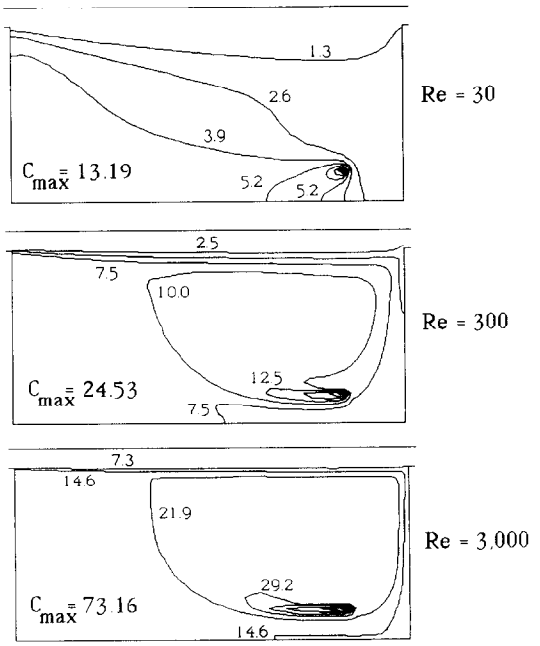

FIG. 7. The steady-state concentration field for source location e and configuration 1.

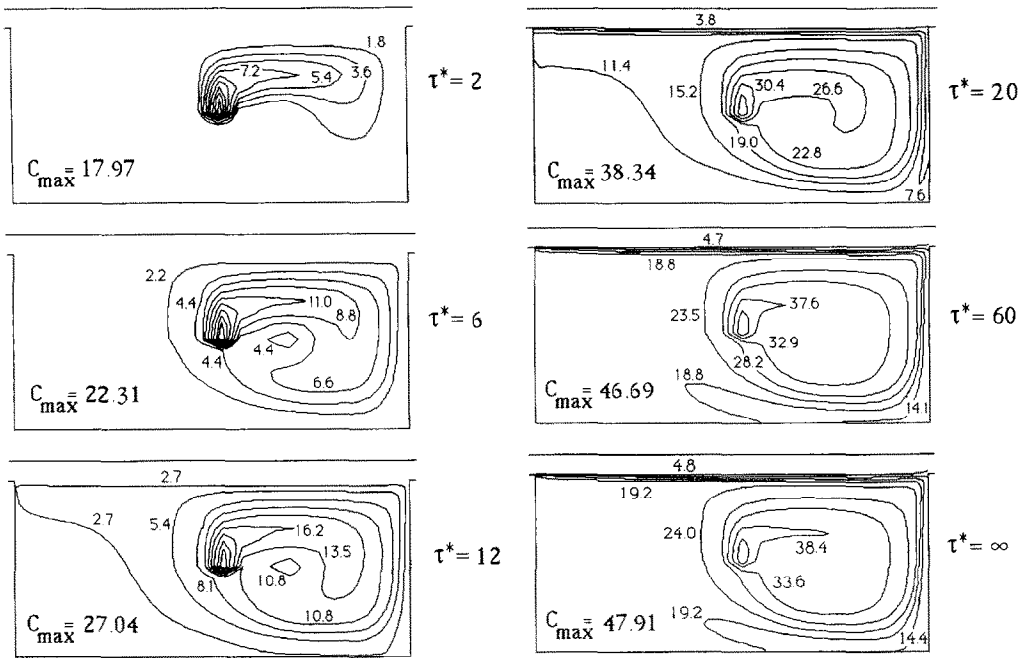

FIG. 8. The time evolution of the contaminant field when the source is positioned in the center of the enclosure ($Re = 3000$, configuration 1).

corresponds to the case when the mass source is located near the outlet (position b), while the lower frame shows the evolution of η_r when the source is located in the center of the enclosure.

Two distinct regimes can be observed in the upper frame of Fig. 9. An initial, almost linear variation of $\eta_r(\tau^*)$ prevails when the contaminant is carried away by the jet, and the removal efficiency increases abruptly. Note that when $Re = 30$ the source is located inside the jet path (Figs. 2 and 4). As the Reynolds number increases, and the jet path becomes straighter, the source ends up inside the clockwise cell, thus causing a significant reduction in the rate of removal of contaminant. The second regime is dominated by the diffusion of mass through the jet shear layer. In this second regime the η_r increase is considerably slower.

The lower frame of Fig. 9 shows a similar behavior, however in this case the source is located further from the jet. As the clockwise cell grows stronger with the increasing Reynolds number, the contaminant becomes trapped more effectively in the lower region of the enclosure. Figure 10 illustrates the same effect in terms of the volume-averaged concentration $\bar{C}$. The averaged concentration for $Re = 3000$ in the steady state is one order of magnitude greater than for $Re = 30$. This result is important, because it shows that for a certain configuration a cleaner steady-state

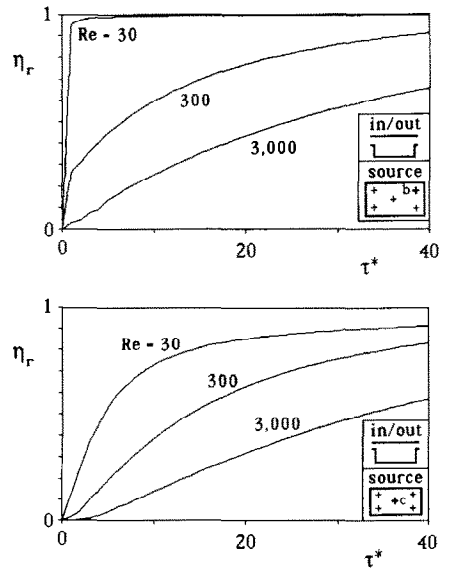

FIG. 9. The time evolution of the removal efficiency: the effects of the Reynolds number and the source location (configuration 1).

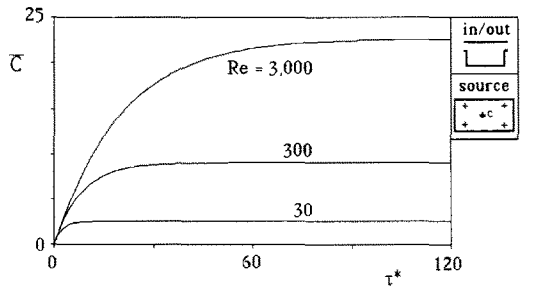

FIG. 10. The time evolution of the volume-averaged concentration (configuration 1, source position c).

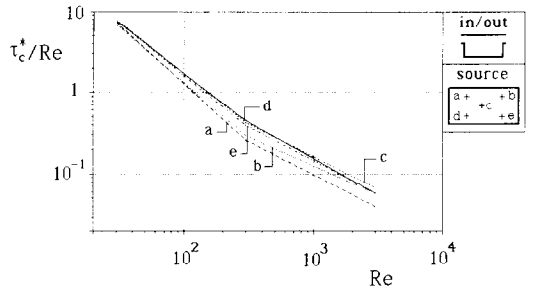

FIG. 11. The critical time for five source locations in configuration 1.

enclosure can be achieved with a slower through flow (lower Reynolds number).

The critical removal time is determined when the amount of contaminant that is being generated inside the cavity approaches within 0.001% of the amount that is being carried away by the ventilation system

$$1-\eta_r(\tau_c^*) = 10^{-5}. \tag{26}$$

It is important to note that the actual critical time t_c (s) that corresponds to the dimensionless time τ_c^* decreases as Re increases

$$t_c = \frac{\tau_c^*}{Re}\frac{HL}{v}. \tag{27}$$

In other words, the ratio τ_c^*/Re is a dimensionless measure of the actual critical time t_c. This ratio is reported in Fig. 11, which shows that the critical time decreases monotonically as Re increases. For instance, with the source located at the center of the enclosure (position c), the actual critical time (τ_c^*/Re) decreases from 7.76 at $Re = 30$ to 0.423 at $Re = 300$, and to 0.067 at $Re = 3000$.

5. THE EFFECT OF CHANGING THE INLET/OUTLET CONFIGURATION

Figure 12 shows the steady-state flow fields in the remaining inlet/outlet configurations (namely, configurations 2–4). In all cases, the Reynolds number is 3000. As in configuration 1, a major clockwise cell occupies most of the enclosure, while smaller cells persist near the corners and the inlet region.

The steady-state concentration fields in configurations 2–4 can be compared by viewing Figs 13–16. Each figure represents a case in which the mass source is located near one of the corners of the enclosure (i.e. source positions a, b, d and e). The Reynolds number is 3000 in all the figures.

An interesting contaminant 'trapping' effect becomes visible as we compare frame-by-frame Figs. 12 and 13. In configuration 4 (the bottom frames) the jet is L-shaped, and most of the enclosure is occupied by a counterclockwise roll. Due to this roll, when the mass source is located as in Fig. 13 (i.e. position a), the contaminant is trapped in the enclosure. Note that

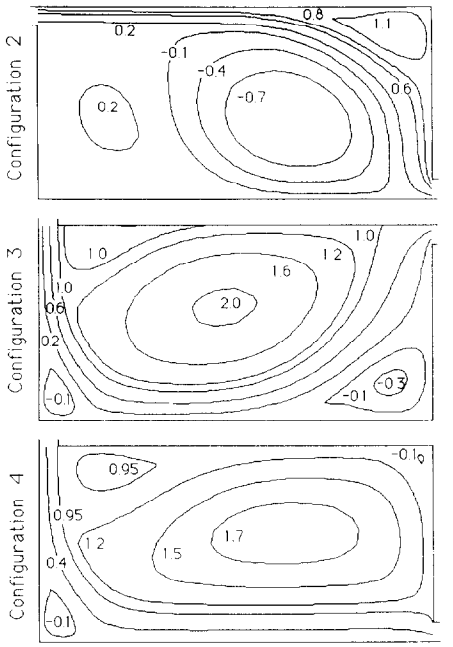

FIG. 12. The steady-state flow field for inlet/outlet configurations 2–4 ($Re = 3000$).

in the lower frame of Fig. 13 the maximum concentration is three times greater than in configurations 2 and 3. A similar effect is visible in the upper frame of Fig. 15, and in the middle frame of Fig. 16.

The time-dependence of the removal efficiency in all four inlet/outlet configurations is summarized in

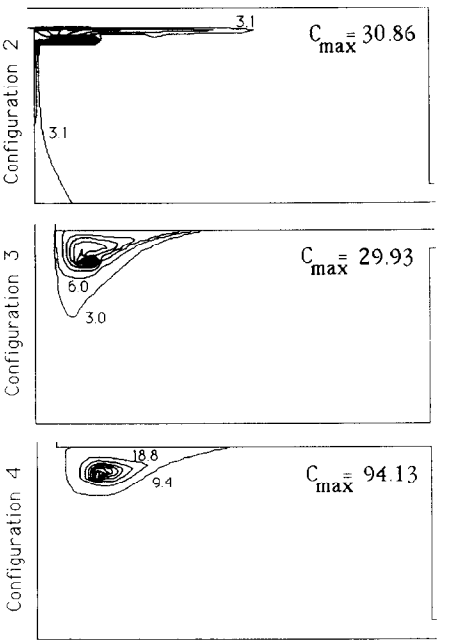

FIG. 13. The steady-state concentration field for source location a ($Re = 3000$).

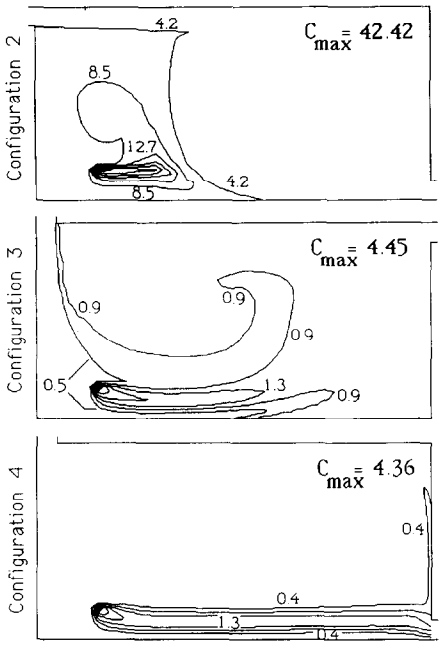

FIG. 14. The steady-state concentration field for source location b ($Re = 3000$).

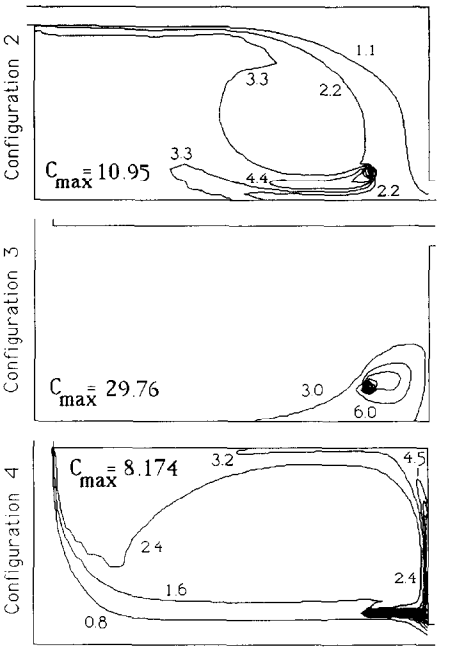

FIG. 16. The steady-state concentration field for source location e ($Re = 3000$).

Fig. 17. Only two source locations are represented by these graphs, the lower-left corner (d) and the center (c). A first observation is that in configuration 1 the removal efficiency is nearly zero during an initial time interval. This behavior is due to the large distance between the in–out jet and the source, when the concentration in the rotating cell must reach a certain level before it can cross the shear layer, into the jet region.

The lower graph of Fig. 17, shows that when the source is located in the center of the enclosure some of the $\eta_r(\tau^*)$ curves cross over. In configuration 4, for example, the removal efficiency exceeds that of configurations 2 and 3 when $\tau^* \gtrsim 50$. This change in behavior is due to the fact that in time the con-

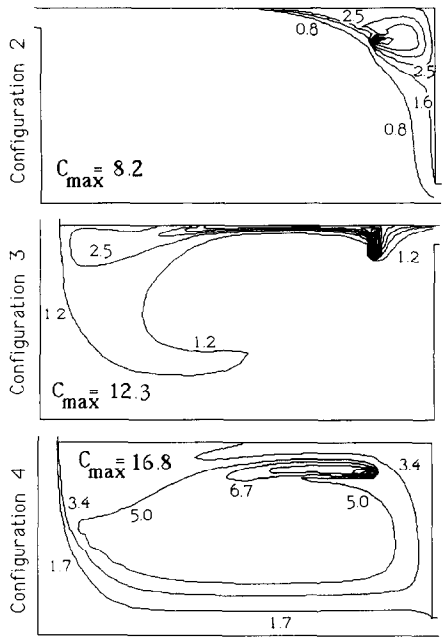

FIG. 15. The steady-state concentration field for source location d ($Re = 3000$).

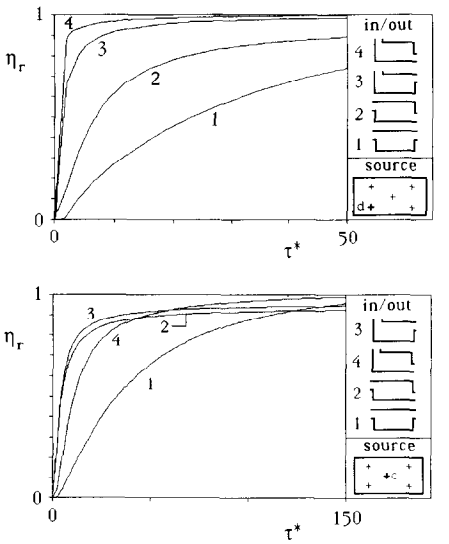

FIG. 17. The effects of inlet/outlet configuration and source location on the time evolution of the removal efficiency ($Re = 3000$).

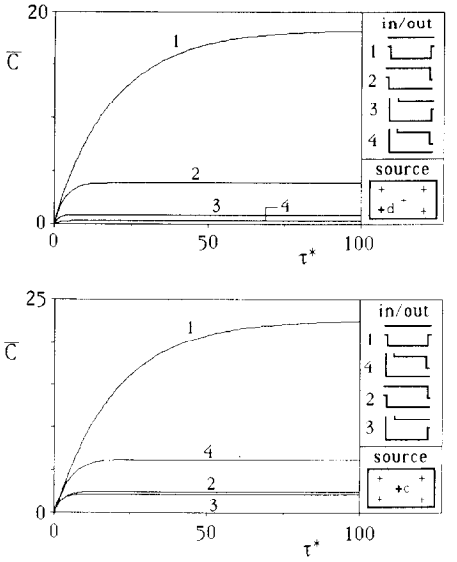

FIG. 18. The effects of inlet/outlet configuration and source location on the time evolution of the volume-averaged concentration ($Re = 3000$).

centration field redistributes itself around the jet stream.

The same set of numerical experiments is summarized in Fig. 18 by using the enclosure-averaged concentration $\bar{C}$. Noteworthy in this figure is that $\bar{C}$ reaches its steady-state value at times τ^* considerably shorter than those needed for reaching the η_r steady state.

The more important conclusion made visible by Fig. 18 is that the lowest steady-state $\bar{C}$ value corresponds to a certain combination of inlet/outlet configuration and source location. In other words, given the source location, there is an optimal positioning of the inlet and outlet ports that guarantees the lowest concentration of contaminant in the steady state. Configuration 4 is the most effective when the source is located in corner d, while configurations 2 and 3 perform almost equally when the source is located in the center. In general, it seems that the most effective inlet/outlet configuration is the one that channels the jet stream through the zone inhabited by the concentrated source of contaminant.

Figure 19 stresses this conclusion, by reporting the steady-state $\bar{C}$ value calculated for all combinations of inlet/outlet configuration and source location. The least effective configuration (highest $\bar{C}$) is configuration 1, in which the jet stream hugs the ceiling and bypasses the source. For that reason, the steady-state $\bar{C}$ value in configuration 1 is almost independent of source location.

The second least effective configuration is 4, in which the jet stream follows the left side and bottom of the enclosure. This configuration is effective only when the source is located near the corner swept by the stream (d).

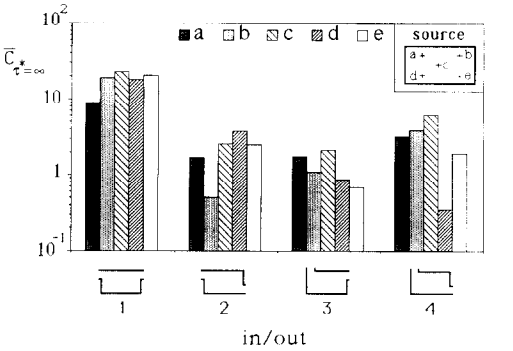

FIG. 19. The steady-state volume-averaged concentration for all the source locations and inlet/outlet configurations ($Re = 3000$).

The most effective configuration (lowest $\bar{C}$) is configuration 3, in which the inlet and outlet are perpendicular and near the same side of the enclosure (the ceiling). In this configuration, the jet stream is forced to follow a longer path through the enclosure, a path that comes near most of the five source locations a–e.

The combinations of inlet/outlet configuration and source location can be ranked also by comparing their respective critical (or cleaning) times, Fig. 20. In general terms, the combinations that yield the lowest steady-state $\bar{C}$ values require some of the longest times. The performance of configuration 1 is again insensitive to the source location. Configuration 3, which is effective for contaminant removal in the steady state, is 'rapid' only when the source is located on the opposite side of the inlet and outlet ports.

6. CONCLUSION

This study showed that the maximum contaminant level in an enclosure can be reduced significantly by properly positioning the inlet and outlet ports. There is an optimal inlet/outlet configuration for each position that the source may occupy inside the enclosure.

When a short contaminant removal time is not a major requirement, slow ventilation schemes can

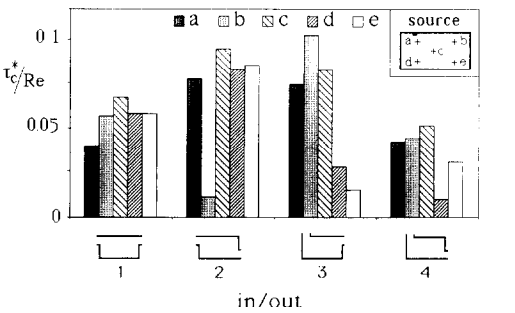

FIG. 20. The critical time for all the source locations and inlet/outlet configurations ($Re = 3000$).

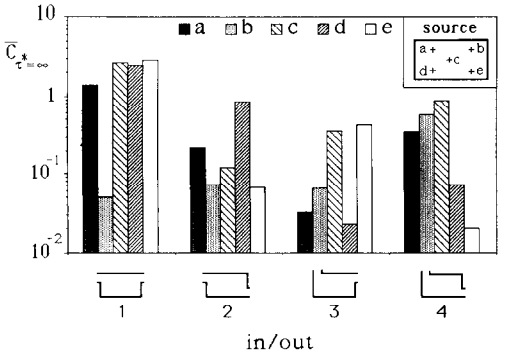

FIG. 21. The steady-state volume-averaged concentration for all the source locations and inlet/outlet configurations ($Re = 30$).

achieve even lower levels of contaminant concentration. Figure 21 shows that when the flow is much slower and laminar ($Re = 30$), the steady-state concentration levels are generally ten times lower than in the $Re = 3000$ flows of Fig. 19. The significant decrease in the steady-state concentration level is accompanied by a 100-fold increase in the critical time needed for reaching the steady state. This secondary effect can be seen by comparing the critical times of Fig. 20 ($Re = 3000$) with those of Fig. 22 ($Re = 30$).

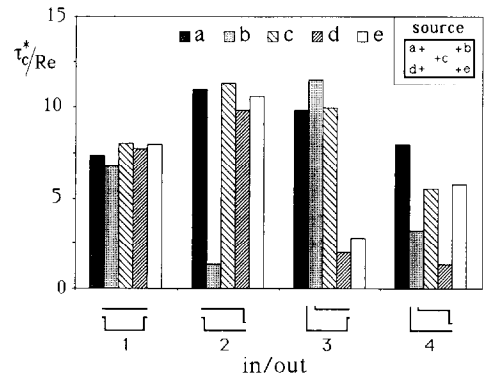

FIG. 22. The critical time for all the source locations and inlet/outlet configurations ($Re = 30$).

Acknowledgement—This work was supported in part by the DOE Office of Building Technology, Division of Building Systems, John Talbott, Program Manager. The numerical work was conducted using the Cornell National Supercomputer Facility, a resource of the Center for Theory and Simulations in Science and Engineering (Cornell Theory Center), which receives major funding from the National Science Foundation and IBM Corporation, with additional support from New York State and members of the Corporate Research Institute.

REFERENCES

1. W. P. Jones and B. E. Launder, The prediction of laminarization with a two-equation model of turbulence, *Int. J. Heat Mass Transfer* **15**, 301–314 (1972).
2. S. V. Patankar, E. M. Sparrow and M. Ivanovic, Thermal interactions among the confining walls of a turbulent recirculating flow, *Int. J. Heat Mass Transfer* **21**, 269–274 (1978).
3. J. L. Lage, A. Bejan and R. Anderson, Efficiency of transient contaminant removal from a slot ventilated enclosure, *Int. J. Heat Mass Transfer* **34**, 2603–2615 (1991).
4. R. Anderson and M. Mehos, Evaluation of indoor air pollutant control techniques using scale experiments, *Engineering Solutions to Indoor Air Problems, Proc. ASHRAE Conf. IAQ 88*, Atlanta, Georgia, pp. 193–208 (1988).
5. V. Hlavacek and J. Votruba, Steady-state operation of fixed-bed reactors and monolithic structures. In *Chemical Reactor Theory, A Review* (Edited by L. Lapidus and N. R. Amundson), pp. 314–404. Prentice-Hall, Englewood Cliffs, New Jersey (1977).
6. D. Schmal, J. H. Duyzer and J. van Heuven, A model for the spontaneous heating of coal, *Fuel* **64**, 963–972 (1985).
7. T. Handa, M. Morita, O. Sugawa, T. Ishii and K. Hayashi, Computer simulation of the spontaneous combustion of coal storage, *Fire Sci. Technol.* **3**, 13–24 (1983).
8. J. E. Gatica, H. J. Viljoen and V. Hlavacek, Interaction between chemical reaction and natural convection in porous media, *Chem. Engng Sci.* **44**, 1853–1870 (1989).
9. S. V. Patankar, *Numerical Heat Transfer and Fluid Flow*. Hemisphere, Washington, DC (1980).

ENLEVEMENT DE CONTAMINANT GENERE PAR UNE SOURCE DISCRETE DANS UNE CAVITE VENTILEE PAR UNE FENTE

Résumé—On rapporte les résultats d'une étude numérique de l'enlèvement, variable dans le temps, d'un contaminant pour une cavité bidimensionnelle avec une entrée et une sortie. Le contaminant est libéré, à partir du temps $t = 0$, par une source concentrée située dans la cavité. Ce contaminant est enlevé par un écoulement de traverse entre entrée et sortie. On couvre les régimes d'écoulement laminaire et turbulent représentés par $30 \leqslant Re \leqslant 3000$, où Re est le nombre de Reynolds basé sur la largeur d'entrée et la vitesse moyenne. L'enlèvement du contaminant est caractérisé par l'efficacité η_r, la concentration moyenne de contaminant $\bar{C}$ et le temps critique t_c (lavage). On considère les effets de Re, de l'orientation du jet de ventilation et de l'emplacement de la source. On montre que le mouvement et la distribution du contaminant sont compliqués et qu'ils dépendent fortement de la position de la source. On montre aussi comment le positionnement relatif des fentes et de la source influence le mécanisme d'enlèvement du contaminant. La configuration optimale associée avec chaque position de la source est rapportée. Des cas de ventilation faibles peuvent conduire à des niveaux très bas de contaminant lorsqu'un temps court d'enlèvement de contaminant n'est pas exigé.

ENTFERNUNG VON VERUNREINIGUNGEN AUS EINER PUNKTFÖRMIGEN QUELLE IN EINEM DURCH SCHLITZE BEFLÜFTETEN BEHÄLTNIS

Zusammenfassung—Es werden die Ergebnisse einer numerischen Untersuchung über die zeitlich veränderliche Entfernung von Verunreinigungen aus einem zweidimensionalen Behältnis mit je einem Ein- und Ausgang vorgestellt. Die Verunreinigungen werden ab einem bestimmten Zeitpunkt von einer punktförmigen Quelle innerhalb des Behältnisses freigesetzt. Durch die Durchströmung zwischen Ein- und Auslaß wird die Verunreinigung entfernt. Die untersuchte Strömung umfaßt den laminaren und turbulenten Bereich mit Reynolds-Zahlen im Bereich $30 \leqslant Re \leqslant 3000$, wobei die Reynolds-Zahl mit der Eintrittsbreite und der mittleren Geschwindigkeit gebildet wird. Die Wirksamkeit des Reiningungsprozesses wird mit Hilfe des Reinigungs-Wirkungsgrades η_r, der volumengemittelten Konzentration der Verunreinigung $\bar{C}$ und der kritischen Reinigungszeit t_c beschrieben. Der Einfluß der Reynolds-Zahl, der Orientierung des Lüftungsstrahls und der Quellenplazierung wird dargestellt. Es zeigt sich, daß die Bewegung und die Verteilung der Verunreinigung sehr komplex ist und stark von der Plazierung der Quelle abhängt. Außerdem wird aufgezeigt, wie die relative Lage von Ein- und Auslaß einerseits und Quelle andererseits den Reinigungsvorgang beeinflußt. Die optimale Plazierung des Ein- und Auslasses für jede Position der Punktquelle wird beschrieben. Eine langsamere Durchströmung kann zu geringeren Konzentrationen der Verunreinigung führen, wenn die Zeit bis zur Entfernung der Verunreinigung kein wesentliches Kriterium darstellt.

УДАЛЕНИЕ ПРИМЕСИ, ОБРАЗУЕМОЙ ДИСКРЕТНЫМ ИСТОЧНИКОМ В ПОЛОСТИ С ПРОДУВАЕМЫМИ ЩЕЛЯМИ

Аннотация—Представлены результаты численного исследования зависящего от времени удаления примеси из двумерной полости с одним входом и одним выходом. Образование примеси начинается в момент времени $t = 0$ за счет сосредоточенного источника, находящегося в полости. Удаление примеси осуществляется сквозным потоком между входным и выходным отверстиями. Исследуются ламинарный и турбулентный режимы течения, соответствующие $30 \leqslant Re \leqslant 3000$, где Re – число Рейнольдса, определяемое шириной входного отверстия и средней скоростью. Эффективность схемы удаления примеси выражается через коэффициент удаления η_r, усредненную по объему концентрацию примеси $\bar{C}$ и критическое время t_c, соответствующее полному удалению примеси. Обсуждается влияние Re, ориентации вентилирующей струи и расположения источника. Найдено, что движение и распределение примеси являются сложными и существенно зависят от размещения источника. Показано также, каким образом относительное расположение отверстий и размещение источника оказывают влияние на процесс удаления примеси. Описывается оптимальная конфигурация входа и выхода в зависимости от расположения источника примеси. Использование схем медленной вентиляции может привести к более низким уровням примеси, если быстрота ее удаления не является основным требованием.